Fusion and quasi-elastic scattering in the ^{6,7}Li + ^{197}Au systems

C. S. Palshetkar,[1] Shital Thakur,[1] V. Nanal,[1,*] A. Shrivastava,[2] N. Dokania,[3,4] V. Singh,[3,4] V. V. Parkar,[2] P. C. Rout,[2] R. Palit,[1] R. G. Pillay,[1] S. Bhattacharyya,[5] A. Chatterjee,[2] S. Santra,[2] K. Ramachandran,[2] and N. L. Singh[6]

[1]*Department of Nuclear and Atomic Physics, Tata Institute of Fundamental Research, Mumbai 400 005, India*

[2]*Nuclear Physics Division, Bhabha Atomic Research Centre, Mumbai 400 085, India*

[3]*India-based Neutrino Observatory, Tata Institute of Fundamental Research, Mumbai 400 005, India*

[4]*Homi Bhabha National Institute, Anushaktinagar, Mumbai 400 094, India*

[5]*Variable Energy Cyclotron Centre, Kolkata 700 064, India*

[6]*Department of Physics, M. S. University of Baroda, Vadodara 390 002, India*

(Received 30 October 2013; revised manuscript received 7 January 2014; published 13 February 2014)

Fusion and quasi-elastic scattering measurements have been carried out for ^{6,7}Li + ^{197}Au systems in the energy range $E/V_b \sim 0.7$ to 1.5. Coupled-channel calculations including coupling to inelastic states of the target and projectiles are able to explain an enhancement in measured fusion cross sections at energies below the barrier. At energies above the barrier the complete fusion cross sections are found to be suppressed compared to the coupled-channel predictions for both systems. A systematic comparison of fusion cross sections of the weakly bound stable nuclei ^{6,7}Li and halo nuclei ^{6,8}He on a ^{197}Au target is presented. Barrier distributions from quasi-elastic scattering are seen to shift towards higher energies with respect to fusion after inclusion of the breakup-α channel for both ^{6}Li and ^{7}Li.

DOI: 10.1103/PhysRevC.89.024607 PACS number(s): 25.70.Jj, 25.70.Bc

I. INTRODUCTION

Reactions with weakly bound stable and unstable nuclei have been rigorously studied in recent years. The low binding energies of these nuclei, leading to a significant effect of the coupling to continuum on different reaction channels, have been the main driving force in such studies. In addition, radioactive ion beams are found to exhibit unusual features such as halo and skin structures, extended shapes, and large breakup probabilities [1–3]. The effect of breakup on different reaction channels has been primarily studied via fusion and elastic scattering. In the case of fusion of weakly bound nuclei, both complete fusion (CF)—where the whole of the projectile fuses with the target—and incomplete fusion (ICF)—where after breakup of the projectile one of the fragments fuses with the target—are possible. In the case of reactions with neutron-rich radioactive ion beams, the coupling to transfer is also found to be important [2]. Recent results in the ^{8}He + ^{197}Au reaction indicate that the sub-barrier total reaction cross section is dominated by direct reactions, in the form of one- and two-neutron stripping [4]. In the case of weakly bound stable nuclei, it has been observed that CF cross sections at above-barrier energies are suppressed compared to calculations which do not include the effect of breakup coupling [1,2].

The coupling between different reaction channels leads to a distribution of barriers rather than a single barrier [5]. It was proposed that such a distribution could be experimentally obtained from high-precision fusion cross sections ($\sigma_{\rm fus}$) [6]. The sensitivity of the fusion data to the coupling of different reaction channels can be efficiently investigated through the fusion barrier distribution, as it involves the second derivative of fusion cross sections. In addition, the potential parameters used in theoretical calculations can be constrained by choosing a set of parameters which are able to reproduce the barrier distribution as accurately as possible. However, a measurement of very precise fusion cross sections is required to obtain a reliable barrier distribution. Also, the second derivative involved in obtaining the distribution leads to larger errors at energies above the barrier in extracting the distribution. Alternatively, it was proposed that a similar distribution can be obtained from backward-angle quasi-elastic (QEL) scattering [7]. In this case the first derivative of the ratio of the QEL scattering to the Rutherford cross section is taken as a function of the center-of-mass energy of the projectile. The incoming flux that penetrates the barrier corresponds to the transmission (T) through the barrier, while the flux scattering from the barrier corresponds to the reflection (R) at the barrier. Owing to conservation of the reaction flux, the fusion and QEL scattering process can be considered complementary and barrier distributions obtained from both types of measurements are expected to be similar [8]. Recently such studies have been carried out using weakly bound stable nuclei [9–15]. In some cases [9,10,13] it has been found that the barrier distribution obtained from QEL scattering including only the elastic + inelastic + transfer channels peaks at a lower energy compared to the corresponding barrier distribution obtained from fusion. It was suggested by Zagrebaev [16] that QEL scattering measurements represent the total reaction threshold distribution rather than the fusion barrier distribution. This would manifest in differences in the barrier distribution obtained from fusion and QEL scattering for tightly bound heavy projectile-target combinations as well as for weakly bound projectiles. Such a discrepancy has been reported in the ^{6}Li + ^{144}Sm system [17].

There are limited measurements to compare fusion and QEL scattering including breakup and it is desirable to

*nanal@tifr.res.in

study both these processes consistently for the same system involving weakly bound nuclei. With this motivation, the excitation function measurements for CF and QEL scattering have been carried out for the projectiles ^{6}Li and ^{7}Li with different breakup thresholds (1.67 and 2.47 MeV, respectively) on an ^{197}Au target over the wide energy range of $0.7 \leqslant E/V_b \leqslant 1.5$. The choice of target was also influenced by the fact that data for fusion of halo nuclei, namely, ^{6}He + ^{197}Au [18] and ^{8}He + ^{197}Au [4], are available. Initial fusion results have been reported in Ref. [19]. This paper presents barrier distributions obtained from both QEL scattering measurements and fusion data. Further, a systematic comparison of fusion cross sections of weakly bound stable nuclei and halo nuclei on ^{197}Au is also presented.

The paper is organized as follows: experimental details of fusion measurement employing the off-line γ-counting technique, online γ-counting for measurement of ICF channels, and QEL scattering for ^{6,7}Li + ^{197}Au systems are given in Sec. II. Fusion excitation functions and barrier distributions obtained from the data along with results of simplified coupled-channel (CC) calculations performed for both systems are given in Sec. III A. A comparison of fusion cross sections of the weakly bound stable nuclei ^{6,7}Li and halo nuclei ^{6,8}He on ^{197}Au target is presented. In addition, excitation functions for the ICF and transfer channels obtained from the off-line as well as the online γ-counting measurement are presented in this section. QEL excitation function and barrier distributions obtained are presented in Sec. III B along with a comparison of the barrier distributions extracted from the fusion and QEL scattering data for ^{6}Li. A summary of both the measurements and the conclusions is presented in Sec. IV.

II. EXPERIMENTAL DETAILS

Fusion and QEL scattering measurements were carried out in separate experiments using ^{6,7}Li beams from the Pelletron Linac facility at TIFR, Mumbai, India. For the fusion measurement, the off-line γ-counting technique was employed. ^{6,7}Li beams of energies between 23 and 44 MeV (in the laboratory frame) were bombarded onto self supporting, rolled ^{197}Au target foils (∼1.5–1.65 mg/cm^2 thick) with beam currents of 10 to 20 pnA. The ^{197}Au foils were backed by aluminum catcher foils (∼3 mg/cm^2 thick) to stop recoiling products. For optimum usage of beam time, some of the irradiations were done using two targets in a cascaded geometry using catcher foils of suitable thickness. In the case of the cascaded target geometry, the incident energy as well as the spread in the energy was calculated using TRIM [20]. In order to correct for fluctuations in the beam currents during irradiation, the integrated current was recorded at intervals of 10–30 s during the entire duration of each irradiation employing a CAMAC-based scaler. The off-line γ counting of irradiated targets was done using two energy- and efficiency-calibrated HPGe detectors. To count the targets irradiated at below-barrier energies, the HPGe detectors were surrounded by a graded shielding consisting of inner layers of Ni + Cd foils followed by an outer layer of 5-cm-thick lead. Data were collected by keeping the irradiated targets at a distance of ∼10 cm from the detector window as well as on-face (especially for sub-barrier energies). Data were recorded using a CAMAC-based acquisition system, LAMPS [21].

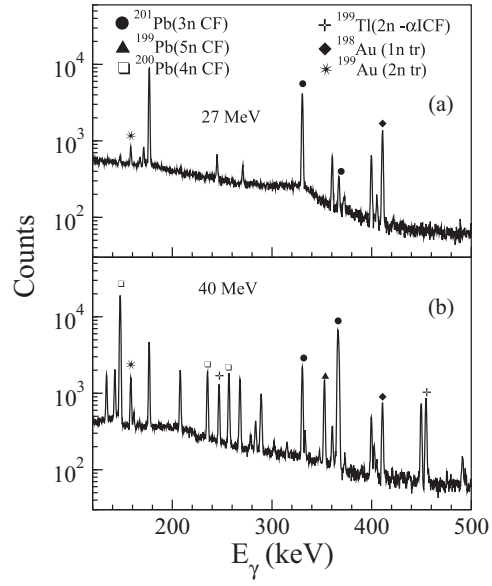

FIG. 1. Typical γ-ray spectrum after irradiation of a ^{197}Au target with a ^{7}Li beam of (a) $E_{\rm lab} = 27$ MeV and (b) $E_{\rm lab} = 40$ MeV. The γ lines corresponding to evaporation residues (ER) from CF ($^{199-201}$Pb), n transfer (^{198,199}Au), and α-ICF (^{199}Tl) identified in the experiment are marked by symbols at the top of the respective peaks.

Typical γ-ray spectra obtained after irradiation of a ^{197}Au target with a ^{7}Li beam of $E = 27$ and 40 MeV are shown in Fig. 1. Gamma rays arising from different reaction channels like CF ($^{199-201}$Pb), n transfer (^{198,199}Au), and α-ICF (^{199}Tl) are clearly seen. Table I summarizes all the channels identified experimentally in ^{6,7}Li + ^{197}Au systems. Half-lives of various γ rays were followed for unambiguous identification of the residues. The cross sections of different channels were extracted from observed γ-ray yields. For many of the decay products, more than one γ ray was observed and extracted cross sections from different γ rays were consistent within a few percent. Only in the case of ^{199}Pb^{g} was the measured $T_{1/2} = 103 \pm 1.4$ min found to be higher, by ∼14%, than the literature value of 90 min [22].

The breakup of ^{6}Li (^{7}Li) into $\alpha + d(t)$ and subsequent $d(t)$ capture by ^{197}Au results in the reaction product ^{199}Hg (^{200}Hg), which further undergoes neutron evaporation to give $^{196-198}$Hg ($^{197-199}$Hg). Both ^{197}Hg and ^{199}Hg have isomeric states and cross sections could be extracted from off-line data neglecting the population to states lying below the isomeric state, which is expected to be small [23,24]. However, both ^{198}Hg and ^{196}Hg are stable and could not be detected via the off-line γ-counting method. Thus, an online γ-counting experiment for 21 to 45 MeV ^{6,7}Li + ^{197}Au (∼1.6 mg/cm^2) was performed using the Indian National Gamma Array (INGA) [25], consisting of 16 Compton suppressed clover detectors for measuring stable products of direct reactions (d/t, xn), and the proton transfer channel. Due to the observed discrepancy in the $T_{1/2}$ of ^{199}Pb^{g}, the cross section of ^{199}Pb was also extracted from

TABLE I. Reaction products identified in off-line measurements with their half-lives ($T_{1/2}$), γ-ray energy (E_γ), and absolute intensities (I_γ). The "Reaction" column is divided into two parts according to the reaction studied and gives the evaporation channels for the corresponding reaction mentioned in the title.

Reaction		Residue	$T_{1/2}$	E_γ	I_γ
^{6}Li + ^{197}Au	^{7}Li + ^{197}Au			(keV)	(%)
ER from CF					
2n	3n	^{201}Pb	9.33 h	331.15	77
				945.96	7.2
3n	4n	^{200}Pb	21.5 h	147.63	38.2
				257.19	4.52
4n	5n	^{199}Pb^g	90 min	353.39	9.57
				720.24	6.5
				1135.04	7.8
		^{199}Pb^m	12.2 min	424.1	10
5n	6n	^{198}Pb	2.4 h	173.4	18.2
				865.3	6
Transfer					
1n stripping	^{198}Au^g	2.695 d	411.8	95.58	
2n stripping	^{199}Au^g	3.139 d	158.4	40	
1n pickup	^{196}Au^g	6.17 d	333.03	22.9	
				355.73	87
Capture					
(d,2n)	(t,3n)	^{197}Hg^m	23.8 h	133.98	33.5
–	(t,1n)	^{199}Hg^m	42.6 min	158.3	52.3
				374.1	13.8
(α,1n)		^{200}Tl^g	26.1 h	367.94	87
(α,2n)		^{199}Tl^g	7.42 h	208.2	12.3
				455.46	12.4

the online measurement [26]. A silicon surface barrier detector was mounted at 30°, which served as a monitor. Efficiency and calibration of the clover array were done using standard ^{152}Eu and ^{133}Ba sources. A typical γ-ray spectrum is shown in Fig. 2 for ^{6}Li at $E_{lab} = 36$ MeV, where lines of interest are indicated. Both single and γ-γ coincidence data were recorded. The coincidence data were mostly used for clear identification of lines of interest, and cross sections have been extracted from singles data. A comparison of cross sections of ^{200}Pb from

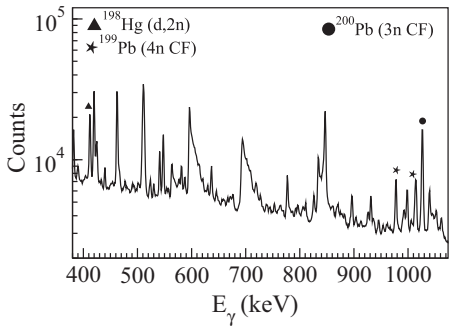

FIG. 2. Typical online γ-ray spectrum for ^{6}Li + ^{197}Au reaction at $E_{lab} = 36$ MeV. The γ lines corresponding to evaporation residues from CF (^{199,200}Pb) and d capture (^{198}Hg) identified in the experiment are marked by symbols at the top of the respective peaks.

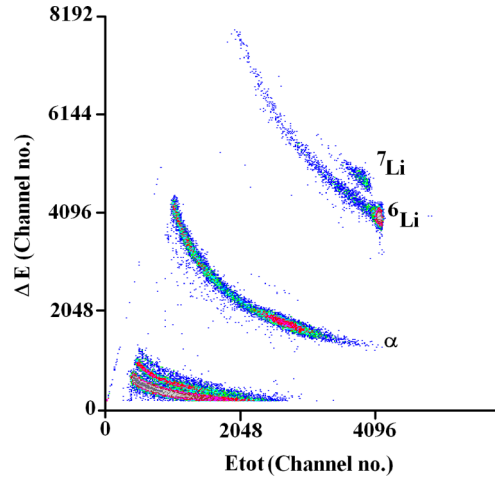

FIG. 3. (Color online) Typical gain-matched ΔE-E spectrum obtained with a ^{6}Li beam for $E = 30$ MeV at a detector angle of 170° (in the laboratory frame).

off-line and online measurements was made and they were found to be consistent within measurement errors.

High-precision QEL scattering measurements were carried out inside a 1-m-diameter scattering chamber having two rotatable arms. Two silicon surface barrier detectors in the ΔE-E telescopic arrangement ($\Delta E \sim 33$ μm thick and $E \sim 2$ mm thick) were mounted on one arm at 150° (T_1) and 170° (T_2), respectively, in order to detect the scattered particles. The angular aperture of the detectors was ~1.1°. Two silicon surface barrier detectors were mounted on the other arm at forward angles of 30° and 40° to serve as monitors. ^{6,7}Li beams ($I \sim 4$–10 pnA) with energies between 23 and 38 MeV in steps of 0.5 MeV were bombarded onto an 800 μg/cm^2 self-supporting ^{197}Au foil. Figure 3 shows a typical gain-matched ΔE-E spectrum obtained in the ^{6}Li + ^{197}Au reaction at 30 MeV.

III. ANALYSIS AND RESULTS

A. Fusion of ^{6,7}Li + ^{197}Au

The evaporation residue excitation function for ^{6,7}Li + ^{197}Au, along with preliminary results for fusion cross section, has been reported in [19]. The CF cross sections for the ^{6,7}Li + ^{197}Au systems obtained by summing all the neutron evaporation channels are shown in Fig. 4. The evaporation residue ^{202}Pb (2n channel), being stable, cannot be detected using the off-line method. However, the contribution from this decay channel is expected to be negligible in the energy region of interest and the same was confirmed during the online measurement. According to the statistical model calculation using PACE [27], the neutron evaporation channels form the dominant part of the fusion cross section (>95%). Only the statistical errors (~3 to 6%) in the CF cross sections have been considered.

The barrier distribution for the ^{6}Li + ^{197}Au system was obtained from the CF cross sections according to the method described in [5] and shown in Fig. 5. The barrier distribution

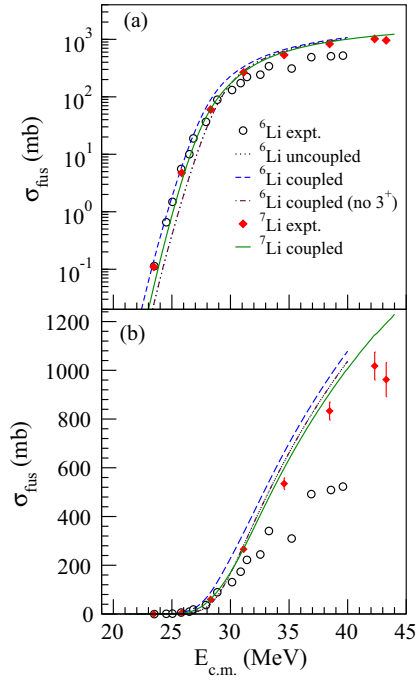

FIG. 4. (Color online) (a) Measured complete fusion excitation function for ^{6,7}Li + ^{197}Au (open and filled symbols, respectively) together with CCFULL calculations. The dashed (solid) line represents the results of CC calculations for ^{6}Li (^{7}Li). Cross sections obtained from CCFULL for ^{6}Li + ^{197}Au without inclusion of the coupling to the 3$^+$ state of ^{6}Li are shown by the dash-dot-dotted line, and those without any coupling are shown by the dotted line. Errors are within the symbol size. (b) Same as (a), but on a linear scale.

for the ^{7}Li + ^{197}Au system could not be extracted from its corresponding fusion cross sections because fewer data points were available for differentiation.

CC calculations for both systems were done using a modified version of the code CCFULL [28], where the effect of ground-state spin is included, in addition to the coupling to the projectile and target excited states. For the projectile

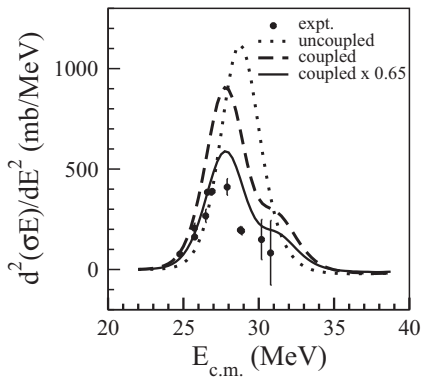

FIG. 5. Barrier distribution for the ^{6}Li + ^{197}Au system. Cross sections obtained from CCFULL without any coupling are shown by the dotted line, whereas the dot-dot-dashed line represents the results of CC calculations. The solid line was obtained by multiplying the CC results by 0.65. Errors are within the symbol size.

couplings, the ground-state deformation was included using the quadrupole moment $Q = -0.0008176$ b for ^{6}Li and –0.0406 b for ^{7}Li [29]. In addition, couplings to the $3^+(E_x = 2.186$ MeV) state with $B(E2\uparrow) = 21.8\,e^2$ fm^4 for ^{6}Li and the $1/2^-$ ($E_x = 0.477$ MeV) state with $B(E2\uparrow) = 8.3\,e^2$ fm^4 for ^{7}Li [30] were also included. The excited states of both ^{6}Li and ^{7}Li were coupled using the rotational coupling scheme. The projection of the angular momentum on the symmetry axis $K = 1^+$ and $K = 3/2^-$ for ^{6}Li and ^{7}Li, respectively, was considered similar to that done in Refs. [30–32]. The excited state of ^{197}Au $E_x = 0.077$ MeV was also coupled as a vibrational state with deformation $\beta = 0.1$ [33]. The Woods-Saxon parameterized Akyuz-Winther potential [34], with $V_0 = 47.34$ MeV, $r_0 = 1.17$ fm, and $a_0 = 0.62$ fm for the ^{6}Li + ^{197}Au system and $V_0 = 47.31$ MeV, $r_0 = 1.17$ fm, and $a_0 = 0.60$ fm for the ^{7}Li + ^{197}Au system, was used for the calculations. For ^{6}Li, the depth of the potential was varied to $V_0 = 58.34$ MeV, keeping the r_0 and a_0 values fixed so as to get the best fit to the barrier distribution, while for ^{7}Li the default potential values gave a satisfactory fit to the data. Results from the CC calculations are plotted in Fig. 4 [dashed line (solid line) for ^{6}Li (^{7}Li)]. CC calculations without any coupling (dotted line) and without coupling to the 3$^+$ state of the ^{6}Li state (dot-dash-dotted line) are also shown for comparison. It can be clearly seen that the coupling to the 3$^+$ state of ^{6}Li (dashed line) is important and results in a large enhancement. Suppression of the experimental CF cross sections compared to the CC calculations has been observed for both systems at the above barrier energies. The observed suppression factor of 0.65 ± 0.23 for ^{6}Li + ^{197}Au is consistent with results obtained for ^{6}Li-induced fusion on heavy targets [35–37]. The uncertainty in the suppression factor is estimated from the uncertainty in the fusion cross sections. We note here that the CF cross sections for the ^{7}Li + ^{197}Au system show a smaller suppression (0.85 ± 0.04) compared to the ^{6}Li + ^{197}Au system and other measurements on heavy targets [35,37].

The barrier distribution extracted from the CC calculations for the ^{6}Li + ^{197}Au system with coupling (dashed line) and without coupling (dotted line) are shown in Fig. 5. The solid line was obtained by multiplying the CC results by the observed suppression factor (0.65). It can be seen that the barrier distribution exhibits a structure with a peak at 28.0 MeV and a shoulder at 31.5 MeV. The data show a good agreement with the calculated distribution.

In addition, cross sections for neutron transfer, $d(t)$ capture, and α capture were obtained from the data and are plotted in Fig. 6 for ^{6}Li and ^{7}Li. The α capture leads to the formation of Tl isotopes, which can also be produced by decay of Pb isotopes, i.e., evaporation residues of the CF. The cross section of α capture for both projectiles was calculated after correcting for the contribution from Pb decay. The dominant γ rays from ^{196}Hg [^{6}Li(d,3n) channel] were mixed up with background/other channels and the cross section could not be cleanly extracted. Similarly in γ-γ coincidence data the 355.7- and 521.2-keV lines of ^{196}Pt, resulting from the proton capture on ^{7}Li, were weakly visible but both γ rays were mixed with strong background lines in singles data. Experimentally the $d(t)$ or α capture could not be distinguished from the direct

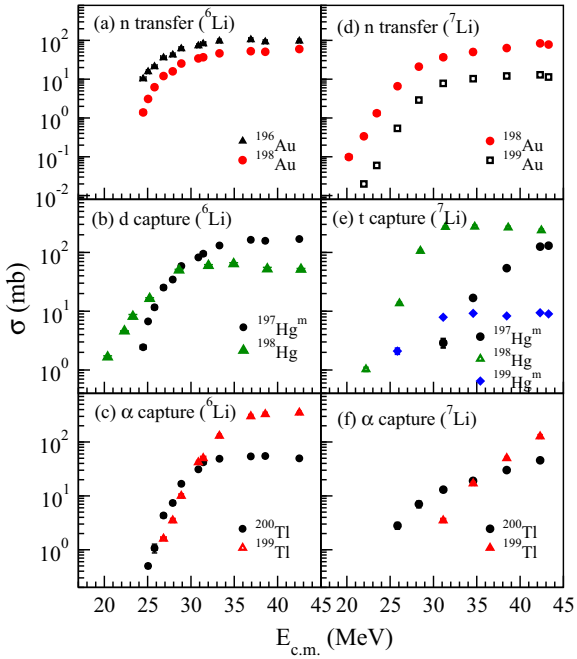

FIG. 6. (Color online) Measured cross sections for n transfer, d capture, and α capture for ^{6}Li + ^{197}Au [panels (a)–(c)] and for ^{7}Li + ^{197}Au [panels (d)–(f)] systems. Different residues, ^{196,198,199}Au, ^{197,198,199}Hg, and ^{199,200}Tl, are indicated in each panel.

transfer of d, t, or α particles. It can be seen that in both systems ICF channels are dominant over n transfer.

For comparison of fusion of weakly bound nuclei with halo nuclei with a ^{197}Au target, scaled cross sections were obtained using the procedure described in Ref. [38], taking into account experimental values of the fusion cross section and height, radius, and curvature of the barrier. Figure 7 shows a systematic comparison of the present data with ^{6,8}He on ^{197}Au from Refs. [4] and [18]. The ^{6,7}Li+^{198}Pt [32,39] data are also shown in the same figure. The scaled cross sections for ^{6,7}Li on ^{197}Au and

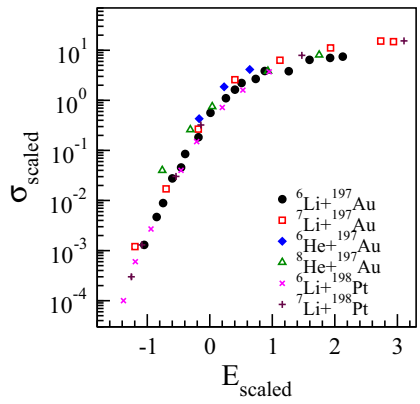

FIG. 7. (Color online) Comparison of scaled fusion cross sections (adopted from [38]) for the present data on ^{6,7}Li + ^{197}Au [19] and ^{6}He + ^{197}Au [18], ^{8}He + ^{197}Au [4], ^{6}Li + ^{198}Pt [32], and ^{7}Li + ^{198}Pt [39] reactions. The quantities σ_{scaled} and E_{scaled} are dimensionless as defined in [38].

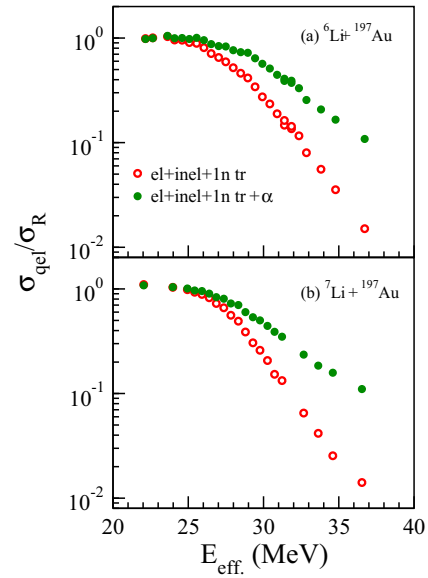

FIG. 8. (Color online) Ratio of the quasi-elastic scattering cross section (obtained from telescope T_2 kept at a 170° laboratory angle) to the Rutherford cross -section for (a) ^{6}Li + ^{197}Au and (b)^{7}Li + ^{197}Au systems. Open and filled circles are for data corresponding to elastic + inelastic + 1n transfer and elastic + inelastic + 1n transfer + α, respectively. Errors are within the symbol size.

^{198}Pt are very similar, indicating no significant target/projectile dependence. Similar results showing no target dependence have been reported in [31] and [37]. A large enhancement of the scaled fusion cross section for halo nuclei ^{6,8}He compared to the weakly bound nuclei (^{6,7}Li) is clearly seen at sub-barrier energies. This could be attributed to the effect of the extended shape of ^{6,8}He and coupling to n transfer.

B. Quasi-elastic scattering in ^{6,7}Li + ^{197}Au and comparison of barrier distributions

The high-precision QEL excitation functions for the ^{6,7}Li + ^{197}Au systems have been extracted from the data collected at 170° and 150°. In these systems the compound nucleus evaporation α is expected to be negligible. The observed α particles in the kinematic window of $E_\alpha = 0.4$–0.7 E_{inc} mainly originate from ICF, non-capture breakup, or transfer followed by breakup and are referred to as breakup α particles in this work. Figure 8 shows the excitation functions for elastic + inelastic + 1n transfer and elastic + inelastic + 1n transfer + α from the 170° data. In obtaining the excitation functions for both systems, the energy was corrected for the energy loss at half the target thickness and the centrifugal correction as done in [7]. The errors in the cross sections, statistical in nature, are of the order ∼1%. For both systems, barrier distributions (D_{qel}) from the QEL scattering excitation function have been extracted taking the interval for the point difference to be 2 MeV. Figure 9 shows a comparison of D_{qel} together with D_{fus} obtained from CC calculations (solid line) and from uncoupled calculations (dotted line). The experimental barrier distribution obtained from the CF cross sections for the ^{6}Li + ^{197}Au system (D_{fus} expt, plotted in

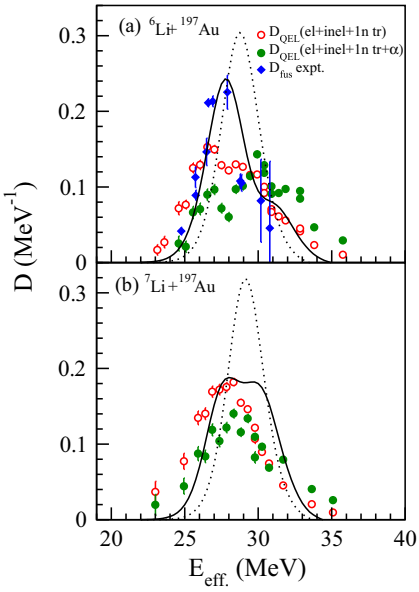

FIG. 9. (Color online) Comparison of the barrier distribution obtained from the quasi-elastic excitation function (filled and open circles) with and without the inclusion of breakup α particles extracted from data obtained from T_2 at 170° for (a) ^{6}Li + ^{197}Au and (b) ^{7}Li + ^{197}Au systems. The dotted line represents the calculated cross sections without any coupling, while the solid line represents the calculated cross sections obtained from CC calculations described in the text. The D_{fus} for ^{6}Li + ^{197}Au, the barrier distribution obtained from the CF excitation function, is also shown in (a) for comparison (filled diamonds).

Fig. 5), normalized by $1/(\pi R_b^2)$ obtained from the intercept found by plotting σ_{fus} versus $1/E_{c.m.}$ at above-barrier energies, is also shown. The peak in D_{qel} appears to be around ∼27 MeV with a shoulder of ∼30 MeV. The QEL barrier distribution appears to be broader and shifted towards a lower energy with respect to D_{fus}. This observation is consistent with those in Refs. [9] and [17]. It should be mentioned that data from the 150° detector also show similar results. By adding the α channel, an attempt was made to understand the effect of the breakup channel on the barrier distribution. For both ^{6,7}Li + ^{197}Au systems, the barrier distribution from the QEL measurement shows a shift towards a higher energy with inclusion of the α channel. The peaks of D_{fus} and D_{qel} including α are different for the present system, unlike in Ref. [9]. Therefore it appears that reaction mechanisms contributing to α particles need to be investigated in detail for comparing D_{fus} and D_{qel} including α.

IV. SUMMARY AND CONCLUSIONS

The fusion and QEL excitation functions for ^{6,7}Li + ^{197}Au systems at energies around the Coulomb barrier have been measured. Fusion cross sections show enhancement below the barrier for reactions with weakly bound projectiles compared to the one-dimensional barrier penetration model. CC calculations including coupling to inelastic excitation of the target and projectiles are able to explain the data reasonably well at below-barrier energies. Experimental fusion cross sections are observed to be suppressed, for both systems, at above-barrier energies compared to the CC calculations. A comparison of scaled fusion cross sections for ^{6,8}He and ^{6,7}Li clearly shows a large enhancement for halo nuclei compared to ^{6,7}Li. For the ^{6}Li + ^{197}Au system, the D_{qel} obtained from the elastic + inelastic + $1n$ transfer cross sections is broader and shifted towards a lower energy compared to the D_{fus}. Barrier distributions from QEL scattering are seen to shift towards a higher energy with inclusion of the breakup-α channel for both ^{6,7}Li. This result is consistent with the interpretation of Zagrebaev [16] that QEL scattering measurements represent the total reaction threshold, which will reflect in differences in the barrier distributions obtained from CF and QEL. It would be interesting to study the effect of breakup on fusion and QEL at energies around the barrier with second-generation RIB facilities, which will deliver high-intensity beams of weakly bound unstable nuclei.

ACKNOWLEDGMENTS

The authors would like to thank the Pelletron Linac Facility staff for smooth operation of the machine during the experiment, Ms. Deepa Thapa and Mr. A. M. Mahadkar for preparation of the targets, Mr. K. S. Divekar and Mr. M. S. Pose for help during experiments. The INGA Collaboration is partially funded by the Department of Science and Technology (DST), Government of India (Grant No. 1R/S2/PF-03/2003-I). Dr. V. V. Parkar acknowledges the financial support of the INSPIRE, DST.

[1] L. F. Canto, P. R. S Gomes, R. Donangelo, and M. S. Hussein, Phys. Rep. **424**, 1 (2006).
[2] N. Keeley, N. Alamanos, K. W. Kemper, and J. L. Sida, Prog. Part. Nucl. Phys. **59**, 579 (2007).
[3] J. F. Liang, and C. Signorini, Int. J. Mod. Phys. E **14**, 1121 (2005).
[4] A. Lemasson, A. Shrivastava, A. Navin, M. Rejmund, N. Keeley, V. Zelevinsky, S. Bhattacharyya, A. Chatterjee, G. de France, B. Jacquot, V. Nanal, R. G. Pillay, R. Raabe, and C. Schmitt, Phys. Rev. Lett. **103**, 232701 (2009).
[5] M. Dasgupta, D. J. Hinde, N. Rowley, and A. M. Stefanini, Annu. Rev. Nucl. Part. Sci. **48**, 401 (1998).
[6] N. Rowley, G. R. Satchler, and P. H. Stelson, Phys. Lett. B **254**, 25 (1991).
[7] H. Timmers, J. R. Leigh, M. Dasgupta, D. J. Hinde, R. C. Lemmon, J. C. Mein, C. R. Morton, J. O. Newton, and N. Rowley, Nucl. Phys. A **584**, 190 (1995).
[8] E. Piasecki, Ł. Świderski, N. Keeley, M. Kisieliński, M. Kowalczyk, S. Khelbnikov, T. Krogulski, K. Piasecki, G. Tiourin, M. Sillanpää, W. H. Trzaska, and A. Trzcińska, Phys. Rev. C **85**, 054608 (2012), and references therein.

[9] C. J. Lin, H. Q. Zhang, F. Yang, M. Ruan, Z. H. Liu, Y. W. Wu, X. K. Wu, P. Zhou, C. L. Zhang, G. L. Zhang, G. P. An, H. M. Jia, and X. X. Xu, Nucl. Phys. A **787**, 281c (2007).
[10] D. S. Monteiro, O. A. Capurro, A. Arazi, J. O. Fernández Niello, J. M. Figueira, G. V. Martí, D. Martínez Heimann, A. E. Negri, A. J. Pacheco, V. Guimarães, D. R. Otomar, J. Lubian, and P. R. S. Gomes, Phys. Rev. C **79**, 014601 (2009).
[11] S. Mukherjee, B. K. Nayak, D. S. Monteiro, J. Lubian, P. R. S. Gomes, S. Appannababu, and R. K. Choudhury, Phys. Rev. C **80**, 014607 (2009).
[12] D. R. Otomar, J. Lubian, P. R. S. Gomes, D. S. Monteiro, O. A. Capurro, A. Arazi, J. O. Fernández Niello, J. M. Figueira, G. V. Martí, D. Martínez Heimann, A. E. Negri, A. J. Pacheco, V. Guimarães, and L. C. Chamon, Phys. Rev. C **80**, 034614 (2009).
[13] H. M. Jia, C. J. Lin, H. Q. Zhang, Z. H. Liu, N. Yu, F. Yang, F. Jia, X. X. Xu, Z. D. Wu, S. T. Zhang, and C. L. Bai, Phys. Rev. C **82**, 027602 (2010).
[14] K. Zerva, A. Pakou, K. Rusek, N. Patronis, N. Alamanos, X. Aslanoglou, D. Filipescu, T. Glodariu, N. Keeley, M. Kokkoris, M. La Commara, A. Lagoyannis, M. Mazzocco, N. G. Nicolis, D. Pierroutsakou, and M. Romoli, Phys. Rev. C **82**, 044607 (2010).
[15] K. Zerva, A. Pakou, N. Patronis, P. Figuera, A. Musumarra, A. Di Pietro, M. Fisichella, T. Glodariu, M. La Commara, M. Lattuada, M. Mazzocco, M. G. Pellegriti, D. Pierroutsakou, A. M. Sanchez-Benitez, V. Scuderi, E. Strano, and K. Rusek, Eur. Phys. J. A **48**, 102 (2012).
[16] V. I. Zagrebaev, Phys. Rev. C **78**, 047602 (2008).
[17] D. S. Monteiro, P. R. S. Gomes, and J. Lubian, Phys. Rev. C **80**, 047602 (2009).
[18] Yu. E. Penionzhkevich, R. A. Astabatyan, N. A. Demekhina, G. G. Gulbekian, R. Kalpakchieva, A. Kulko, S. M. Lukyanov, E. R. Markaryan, V. A. Maslov, Yu. A. Muzychka, Yu. Ts. Oganessian, R. V. Revenko, N. K. Skobelev, Yu. G. Sobolev, D. A. Testov, and T. Zholdybaev, Eur. Phys. J. A **31**, 185 (2007).
[19] Shital Thakur, Vivek Singh, C. S. Palshetkar, V. Nanal, V. V. Parkar, R. G. Pillay, A. Shrivastava, P. C. Rout, K. Ramachandran, and A. Chatterjee, EPJ Web Conf. **17**, 16017 (2011).
[20] http://www.srim.org
[21] http://www.tifr.res.in/~pell/lamps.html
[22] R. E. Doebler, Thesis, Michigan State University, 1970; B. Singh, Nucl. Data Sheets **108**, 79 (2007).
[23] P. Kemnitz, F. Dönau, L. Funke, H. Strusny, D. Venos, E. Will, G. Winter, and J. Meyer ter Vehn, Nucl. Phys. A **293**, 314 (1977).
[24] D. Mertin, R. Tischler, A. Kleinrahm, R. Kroth, H. Hübel, and C. Günther, Nucl. Phys. A **301**, 365 (1978).
[25] R. Palit, S. Saha, J. Sethi, T. Trivedi, S. Sharma, B. S. Naidu, S. Jadhav, R. Donti, P. B. Chavan, H. Tan, and W. Hennig, Nucl. Instrum. Methods Phys. Res. Sec. A **680**, 90 (2012).
[26] G. Baldsiefen, H. Hubel, W. Korten, D. Mehta, N. Nenoff, B. V. Thirumal Rao, and P. Willsau, Nucl. Phys. A **574**, 521 (1994).
[27] A. Gavron, Phys. Rev. C **21**, 230 (1980).
[28] K. Hagino, N. Rowley, and A. T. Kruppa, Comput. Phys. Commun. **123**, 143 (1999).
[29] J. Cederberg, D. Olson, J. Larson, G. Rakness, K. Jarausch, J. Schmidt, B. Borovsky, P. Larson, and B. Nelson, Phys. Rev. A **57**, 2539 (1998).
[30] C. Beck *et al.*, Phys. Rev. C **67**, 054602 (2003).
[31] M. Dasgupta, P. R. S. Gomes, D. J. Hinde, S. B. Moraes, R. M. Anjos, A. C. Berriman, R. D. Butt, N. Carlin, J. Lubian, C. R. Morton, J. O. Newton, and A. Szanto de Toledo, Phys. Rev. C **70**, 024606 (2004).
[32] A. Shrivastava, A. Navin, A. Lemasson, K. Ramachandran, V. Nanal, M. Rejmund, K. Hagino, T. Ichikawa, S. Bhattacharyya, A. Chatterjee, S. Kailas, K. Mahata, V. V. Parkar, R. G. Pillay, and P. C. Rout, Phys. Rev. Lett. **103**, 232702 (2009).
[33] Xiaolong Huang and Chunmei Zhou, Nucl. Data Sheets **104**, 283 (2005).
[34] R. A. Broglia and A. Winther, *Heavy Ion Reaction Lecture Notes, Vol. I: Elastic and Inelastic Reactions* (Benjamin/Cummings, Reading, MA, 1981), p. 114.
[35] M. Dasgupta, D. J. Hinde, S. B. Moraes, P. R. S. Gomes, R. M. Anjos, R. D. Butt, A. C. Berriman, N. Carlin, C. R. Morton, J. O. Newton, and A. Szanto de Toledo, Phys. Rev. C **66**, 041602(R) (2002).
[36] Y. W. Wu, Z. H. Liu, C. J. Lin, H. Q. Zhang, M. Ruan, F. Yang, Z. C. Li, M. Trotta, and K. Hagino, Phys. Rev. C **68**, 044605 (2003).
[37] P. K. Rath, S. Santra, N. L. Singh, R. Tripathi, V. V. Parkar, B. K. Nayak, K. Mahata, R. Palit, Suresh Kumar, S. Mukherjee, S. Appanbabu, and R. K. Choudhury, Phys. Rev. C **79**, 051601(R) (2009).
[38] L. F. Canto, P. R. S. Gomes, J. Lubian, L. C. Chamon, and E. Crema, J. Phys. G **36**, 015109 (2009).
[39] A. Shrivastava, A. Navin, A. Diaz-Torres, V. Nanal, K. Ramachandran, M. Rejmund, S. Bhattacharyya, A. Chatterjee, S. Kailas, A. Lemasson, R. Palit, V. V. Parkar, R. G. Pillay, P. C. Rout, and Y. Sawant, Phys. Lett. B **718**, 931 (2013).